IEEE Transactions on Aerospace and Electronic Systems, Available online 5 June 2019
DOI: 10.1109/TAES.2019.2921181

Nonlinear Autopilot Design for Endo- and Exo-Atmospheric Interceptor with Thrust-Vector-Control

Ju-Hyeon Hong and Chang-Hun Lee

***Abstract*—This paper proposes an autopilot design for an interceptor with Thrust-Vector-Control (TVC) that operates in the endo- and exo-atmospheric regions. The main objective of the proposed autopilot design is to ensure control performance in both atmospheric regions, without changing the control mechanism. In this paper, the characteristics of the aerodynamic forces in both atmospheric regions are first investigated to examine the issue of the conventional control mechanism at various altitudes. And then, a control mechanism, which can be applied to both atmospheric regions, is determined based on the analysis results. An autopilot design is then followed by utilizing the control mechanism and the feedback linearization control (FBLC) method. Accordingly, the proposed autopilot does not rely on changing the control mechanism depending on flight condition unlike the conventional approach as well as it can adjust the control gains automatically according to the changes of flight operating conditions. In this paper, the robustness of the proposed autopilot is investigated through the tracking error analysis and the relative stability analysis in the presence of model uncertainties. The physical meaning of the proposed autopilot is also presented by comparing to the well-known three-loop control structure. Finally, numerical simulations are performed to show the performance of the proposed method.**

***Index Terms*—Autopilot Design, Thrust-Vector-Control, Nonlinear Control, High Altitude Interceptor.**

I. Introduction

An interceptor controls the flight path angle to reach the desired position, such as the predicted intercept point (PIP), during the mid-course phase. In general, there are two ways to control the flight path angle. First, the flight path angle can be directly controlled by imposing the lateral acceleration [1], [2], because the change of the flight path angle can be provided by the lateral acceleration over the speed from the kinematics relationship. Second, the flight path angle can be indirectly controlled by the attitude angle control [3]–[6]. In this approach, the attitude angle is first adjusted to achieve the desired value of flight path angles. At this time, the flight path angle has an angle error by the angle-of-attack, but the angle error rapidly converges to zero by the aerodynamic mechanism. Eventually, the attitude angle becomes the same as the flight path angle.

For interceptors with TVC, the midcourse guidance is typically performed by the flight path angle control through the attitude angle control (i.e., the second control mechanism). Whereas, for the terminal guidance, the acceleration control is utilized to steer the flight path angle as desired (i.e., the first control mechanism). Also, in this approach, an ad-hoc gain scheduling is applied for both the control mechanisms or structures, and gain sets are scheduled with the Mach number, angle-of-attack, and altitude [7].

In the typical approach, however, there is an issue of degrading control performance, as the engagement altitude becomes wider. Since the aerodynamic force is diluted as the altitude increases, in the exo-atmosphere, it is challenging to control the flight path angle by the attitude angle control approach. This can be attributed to the fact that due to the absence of air density in the exo-atmosphere, the convergence speed of the angle-of-attack by the aerodynamic mechanism is too slow to efficiently adjust the flight path angle. In this case, the autopilot system can improve its efficiency by switching to different control structures at a specific altitude, or by blending different types of actuators [7]–[12]. Namely, in the case of lack of the aerodynamic force, in the exo-atmosphere, controlling the flight path angle by the lateral acceleration caused by the thrust (i.e., the first control mechanism) presents an advantage. Therefore, the change of control mechanism or autopilot configuration is recommended by the change of the altitude. However, even in this case, the mechanism still demonstrates difficulty with regard to the choice of an optimal switching condition. It means that if the same control structure could be utilized for both the endo- and exo-atmospheric regions, the performance degradation due to the switching of the control structure could be avoided.

In order to address this issue, in our previous work [13], we suggested a new nonlinear autopilot for the interceptor with TVC at both the endo- and exo-atmospheric regions. Particularly, it was shown in [13] that, by adopting the acceleration perpendicular to the velocity vector as a controlled output, the proposed control mechanism could be effectively operated by utilizing a combination of the aerodynamic force and the thrust at both the endo-and exo-atmospheric regions. Thus, herein, the proposed autopilot does not rely on changing the control mechanism or the configuration of the control structure depending on flight conditions. Moreover, since the proposed autopilot was based on the nonlinear control methodology, the autopilot can automatically adjust the control gains according to the changes of flight operating conditions. In addition, the physical meaning of control commands can be analyzed intuitively using the error equation, proposed in [14], since the

Ju-Hyeon Hong is with the School of Aerospace, Transport and Manufacturing, Cranfield University, Cranfield MK43 0AL, United Kingdom (email: hong.ju.hyeon11@gmail.com)

Chang-Hun Lee is with Department of Aerospace Engineering, Korea Advanced Institute of Science and Technology(KAIST), Daejeon, 34141, Republic of Korea (email: lckdgns@kaist.ac.kr), Corresponding Author

apparent structure of the proposed autopilot can be rearranged in the same way as the well-known three-loop control structure [1], [14]–[19].

This paper is an extension of the previous work [13]. In the previous work [13], we provided the proposed control structure, without detailed analysis and rationale behind the proposed control structure. Correspondingly, this paper focuses on analyzing the characteristics of the proposed control structure. First, we investigated the problems of the conventional approach, which adopts the attitude angle as a controlled output, to obtain insights into the control mechanism at various altitudes. Second, the tracking error analysis was also performed to investigate the performance of the proposed control structure. In addition, the robustness of the proposed autopilot structure was analyzed by the relative stability analysis with model uncertainties. Finally, nonlinear simulations were performed to show the characteristics of the aerodynamic mechanism and basic properties of the proposed autopilot.

This paper is organized as follows: First, in Section II, with the formulation of missile dynamics, the problem to be considered is stated. Then, in Section III, the proposed control mechanism and the proposed autopilot structure are introduced. Following which, the tracking error analysis with the modeling errors of the proposed autopilot is presented in Section IV. The numerical simulation results are presented to validate the performance of the proposed autopilot in Section V. Finally, the conclusions of this paper are presented in Section VI.

II. Problem Definition

A. Missile Dynamics

In this section, the missile dynamics with TVC is described. First, it is assumed that a missile configuration is symmetric, and a roll motion is stabilized. Under these assumptions, the missile dynamics can be decoupled into two identical channels: pitch and yaw. Accordingly, the pitch motion can only be considered as a representative channel in missile autopilot designs. Note, this separation design concept has been widely accepted for missile autopilot designs in several previous studies [14], [18]–[27].

The coordinate systems $\left(\vec{x}^b, \vec{z}^b\right)$, $(\vec{x}^w, \vec{z}^w)$, and $(\vec{x}^n, \vec{z}^n)$ represent the body frame, wind frame, and local reference frame, respectively. The parameters α, θ, and γ are the angle-of-attack, pitch attitude angle, and flight path angle, respectively. The thrust, length of the moment arm, and deflection angle for TVC are denoted by T, l, and δ_t, respectively. The parameter, denoted by V, represents the speed of the missile. The force and moment equations for the missile in the body frame can be written as follows:

$$\begin{aligned} a_x^b &= a_{aero_x}^b + a_{thrust_x}^b \\ a_z^b &= a_{aero_z}^b + a_{thrust_z}^b \\ M_y^b &= M_{aero_y}^b + M_{thrust_y}^b. \end{aligned} \tag{1}$$

where $a_{aero_x}^b$, $a_{aero_z}^b$, $a_{thrust_x}^b$, and $a_{thrust_z}^b$ represent the aerodynamic accelerations and thrust accelerations. The parameters $M_{aero_y}^b$ and $M_{thrust_y}^b$ represent the aerodynamic moment and thrust moment. The total accelerations and moments can be expressed as follows:

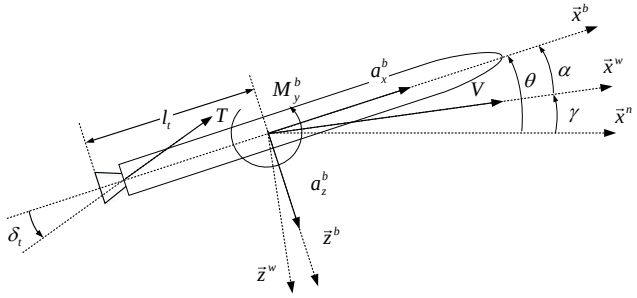

Fig. 1: Missile geometry and parameter definition.

$$\begin{aligned} a_x^b &= \frac{q_\infty S_{ref} C_x\left(M, \alpha, h\right)}{m} + \frac{T}{m}\cos\delta_t \\ a_z^b &= \frac{q_\infty S_{ref} C_z\left(M, \alpha\right)}{m} - \frac{T}{m}\sin\delta_t \\ M_y^b &= q_\infty S_{ref} d_{ref} C_M\left(M, \alpha\right) - l_t T \sin\delta_t. \end{aligned} \tag{2}$$

where $C_x\left(M, \alpha, h\right)$, $C_z\left(M, \alpha\right)$, and $C_M\left(M, \alpha\right)$ are the aerodynamic coefficients. Hereafter, for notational convenience, the aerodynamic coefficients are written in shorthand forms without their arguments. The parameters q_∞, S_{ref}, d_{ref}, and m denote the dynamic pressure, reference area, reference length, and mass, respectively. Thus, the dynamics of the pitch channel can be written as follows:

$$\begin{aligned} \dot{\alpha} &= \frac{-a_x^b \sin\alpha + a_z^b \cos\alpha}{V} + q \\ \dot{q} &= \frac{M_y^b}{I_{yy}}. \end{aligned} \tag{3}$$

where the parameters q and I_{yy} represent the pitch rate and moment of inertia, respectively. By substituting Eq. (2) into Eq. (3), the missile dynamics can be rewritten as

$$\begin{aligned} \dot{\alpha} &= \frac{q_\infty S_{ref}\left(-C_x \sin\alpha + C_z \cos\alpha\right)}{mV} \\ &\quad - \frac{T\left(\sin\alpha\cos\delta_t + \cos\alpha\sin\delta_t\right)}{mV} + q \\ \dot{q} &= \frac{q_\infty S_{ref} d_{ref} C_M}{I_{yy}} - \frac{l_t T \sin\delta_t}{I_{yy}}. \end{aligned} \tag{4}$$

Here, the deflection angle of TVC (i.e., δ_t) can be considered as the control input of the system equation. In the later section, this dynamics equation will be utilized to design the autopilot.

Remark 1. The angle-of-attack α is a purely aerodynamic concept. It is mainly defined in the endo-atmospheric region, and it has no meaning in the exo-atmospheric region. Thus, in the exo-atmospheric region, the parameter α can be considered as the shear angle [28], [29] which represents the angle between the velocity vector and the thrust vector.

B. Problem Statement

In this section, the problem of the conventional approach is discussed. Reiterating, during the midcourse guidance, the

interceptor controls the flight path angle, so that the interceptor reaches the desired position. Then, the interceptor with TVC generally performs the flight path angle control through the attitude angle control. In this approach, the attitude angle θ is first controlled to the desired value of the flight path angle γ_d. When the attitude angle converges to the desired value as $\theta = \gamma_d$, the flight path angle becomes as follows, due to the kinematics relationship $\theta = \alpha + \gamma$ as shown in Fig. 1.

$$\gamma = \gamma_d - \alpha. \tag{5}$$

It means there is a flight path angle error as much as the magnitude of α after performing the attitude angle control. In addition, once $\theta = \gamma_d$, the pitch rate becomes zero as $q = 0$, because γ_d is a constant. In this case, the governing equation of the angle-of-attack Eq. (4) becomes,

$$\begin{aligned}\dot{\alpha} = &\frac{q_\infty S_{ref}\left(-C_x \sin\alpha + C_z \cos\alpha\right)}{mV} \\ &- \frac{T\left(\sin\alpha\cos\delta_t + \cos\alpha\sin\delta_t\right)}{mV}.\end{aligned} \tag{6}$$

Under the small angle approximations of α and δ_t, Eq. (6) can be approximated as follows:

$$\dot{\alpha} \approx \frac{q_\infty S_{ref} C_z}{mV} = \frac{q_\infty S_{ref} C_{z,\alpha}\alpha}{mV}. \tag{7}$$

where $C_{z,\alpha} = \partial C_z / \partial\alpha$. Also, the missile velocity and the parameter $C_{z,\alpha}$ can be assumed as piece-wise constants, since compared to the variable α, in general, they are slowly varying.

In order to investigate the characteristics of the aerodynamic forces in the endo- and exo-atmospheric regions, the behavior of the angle-of-attack can be expressed by the exponential function as follows:

$$\alpha(t) \propto e^{Z_\alpha t}. \tag{8}$$

where the non-dimensional aerodynamic coefficient Z_α is given as:

$$Z_\alpha \triangleq \frac{q_\infty S_{ref} C_{z,\alpha}}{mV}. \tag{9}$$

From Eq. (9), since the aerodynamic coefficient $C_{z,\alpha}$ is always negative, the coefficient Z_α is also negative. Accordingly, from Eq. (8), we can readily observe that the angle-of-attack converges to zero exponentially as $t \to \infty$, and the magnitude of Z_α determines the convergence speed of the angle-of-attack. Then, from Eq. (5), the flight path angle approaches the desired flight path angle (i.e., $\gamma = \gamma_d$), as the angle-of-attack converges to zero. Thus, in this aerodynamic mechanism, the desired flight path angle can be achieved by the attitude angle control.

However, this approach concurrently presents an issue, that is, the performance of flight path angle control by the attitude angle control shows a variance according to the magnitude of Z_α. Since Z_α is given by the function of the dynamic pressure q_∞, as shown in Eq. (8), the magnitude of Z_α exponentially decreases as the altitude increases due to loss of air density. Therefore, the convergence speed of the angle-of-attack decreases significantly in the exo-atmospheric region. As a result, it is readily expected that the flight path angle control through the attitude angle control is ineffective in this region. Namely, there will be a tracking error due to a non-zero angle-of-attack, as shown in Eq. (5), and as such, the interceptor might not accurately reach the desired target position.

In order to address this issue, in the conventional approach, the configuration of the controller is changed from the attitude control mechanism to the lateral acceleration control mechanism after reaching a specific altitude. In other words, the attitude controller could be used in the endo-atmosphere, whereas, the lateral acceleration controller could be utilized in the exo-atmosphere. However, the decision of the specific transition from the attitude control to the acceleration control still becomes an issue concerning the conventional approach and continues to remain ambiguous.

In order to overcome the above issue, in the next section, an autopilot structure for the interceptor, which can be applicable to both the endo- and exo-atmospheres without changing the control configuration will be discussed using the nonlinear control methodology.

III. Nonlinear Autopilot for Interceptor with TVC

This section describes the proposed nonlinear autopilot for the interceptor with TVC. In order to control the flight path angle in both the endo- and exo-atmospheric regions, without changing the control mechanism, the proposed autopilot adopts the normal acceleration, which is perpendicular to the velocity vector, as the controlled output. In addition, to control the normal acceleration, two levels of feedback loops are designed using the feedback linearization control (FBLC) methodology in conjunction with the time-scale separation technique.

A. Proposed Control Mechanism

In order to configure a single controller, which is applicable to both the endo- and exo-atmospheric regions, the basic idea is to select the normal acceleration, which is perpendicular to the velocity vector, as the output variable in both the endo- and exo-atmospheres. As shown in Fig. 1, the acceleration components in the body frame can be transformed into the acceleration components in the wind frame as follows:

$$\begin{bmatrix} a_x^w \\ a_z^w \end{bmatrix} = \begin{bmatrix} \cos\alpha & \sin\alpha \\ -\sin\alpha & \cos\alpha \end{bmatrix} \begin{bmatrix} a_x^b \\ a_z^b \end{bmatrix}. \tag{10}$$

where a_x^w is the acceleration along the velocity vector, and a_z^w is the acceleration perpendicular to the velocity vector, which is the normal acceleration. By utilizing the definition of the normal acceleration, as shown in Eq. (10), the angle-of-attack dynamics can be rewritten as follows from Eq. (3):

$$\dot{\alpha} = \frac{a_z^w}{V} + q. \tag{11}$$

From the kinematics relationship $\theta = \alpha + \gamma$ and Eq. (11), the rate of the flight path angle is determined as

$$\dot{\gamma} = -\frac{a_z^w}{V}. \tag{12}$$

This equation shows that the flight path angle is directly altered by the normal acceleration. From Eqs. (2) and (10), the expression of the normal acceleration is given by

$$a_z^w = \frac{q_\infty S_{ref}\left(-C_x \sin\alpha + C_z \cos\alpha\right)}{m} - \frac{T\left(\sin\alpha\cos\delta_t + \cos\alpha\sin\delta_t\right)}{m}. \tag{13}$$

In the endo-atmosphere, the dominant terms of the normal acceleration in Eq. (13) include the aerodynamic acceleration term with C_z and thrust term with $\cos\delta_t$.

$$a_z^w \approx \frac{q_\infty S_{ref} C_z}{m}\cos\alpha - \frac{T\cos\delta_t}{m}\sin\alpha. \tag{14}$$

As shown in Eq. (14), the normal acceleration is induced by both the aerodynamic force and the thrust in this flight region. In the exo-atmosphere, since the dynamic pressure decreases, the normal acceleration is mostly caused by the thrust term.

$$a_z^w \approx -\frac{T\cos\delta_t}{m}\sin\alpha. \tag{15}$$

Therefore, with the utilization of the normal acceleration as the controlled output, the aerodynamic force and the thrust are naturally combined together. This characteristic is related to the control effectiveness for controlling the normal acceleration.

By taking the time-derivative of a_z^w from Eq. (13), the rate of the normal acceleration is determined as Eq. (16). Note, in this derivation, it is assumed that terms regarding the rate of the deflection angle, $\dot{\delta}_t$, are small.

$$\dot{a}_z^w = -\frac{q_\infty S_{ref} C_{x,\alpha}}{m}\dot{\alpha}\sin\alpha - \frac{q_\infty S_{ref} C_x + T\cos\delta_t}{m}\dot{\alpha}\cos\alpha + \frac{q_\infty S_{ref} C_{z,\alpha}}{m}\dot{\alpha}\cos\alpha - \frac{q_\infty S_{ref} C_z - T\sin\delta_t}{m}\dot{\alpha}\sin\alpha. \tag{16}$$

where $C_{x,\alpha} = \partial C_x/\partial\alpha$. The above equation can be expressed in the general form as

$$\dot{a}_z^w = \eta\frac{d\alpha}{dt} = \left(\eta_A + \eta_T\right)\frac{d\alpha}{dt}. \tag{17}$$

where parameters η_A and η_T are defined as follows:

$$\eta_A = -\frac{q_\infty S_{ref} C_{x,\alpha}}{m}\sin\alpha - \frac{q_\infty S_{ref} C_x}{m}\cos\alpha + \frac{q_\infty S_{ref} C_{z,\alpha}}{m}\cos\alpha - \frac{q_\infty S_{ref} C_z}{m}\sin\alpha. \tag{18}$$

$$\eta_T = -\frac{T\cos\delta_t}{m}\cos\alpha + \frac{T\sin\delta_t}{m}\sin\alpha. \tag{19}$$

Note, the rate of the normal acceleration is directly proportional to the rate of the angle-of-attack, as shown in Eq. (17). Also, this relationship is maintained in both the endo- and exo-atmospheric regions. It means that the normal acceleration can be controlled by the moment control mechanism in both the endo- and exo-atmospheric regions. Specifically, the action of control input introduces the change of the pitch rate (i.e., the generation of moments). On that occasion, the pitch rate causes the change of the angle-of-attack, and the change of the normal acceleration is induced by the change of the angle-of-attack, as shown in Eq. (17). Consequently, a single control structure, which can be used in both environments, is plausible without changing the control mechanism. This reason underpins the proposition for the autopilot to adopt the normal acceleration as the controlled output, in this study.

In this approach, the control mechanism is maintained and only proportional coefficient η changes during the endo- to exo-atmospheric flights. Here, the parameter η physically represents total control effectiveness, and it is composed of the two parameters η_A and η_T, as shown in Eq. (17). These parameters can be considered as the control effectiveness of the normal acceleration control by the aerodynamic force and thrust, respectively. Therefore, we can predict that in this control mechanism, the control force is automatically adjusted from the aerodynamic force and the thrust, considering which is more effective based on the change of flight conditions. Hence, an autopilot designed on this control mechanism does not need to determine the optimal switching condition as mentioned before.

Specifically, under the small angle approximations of α and δ with a small value of C_x, these parameters can be approximated as:

$$\eta_A \approx \frac{q_\infty S_{ref} C_{z,\alpha}}{m}, \quad \eta_T \approx -\frac{T}{m}. \tag{20}$$

In Eq. (20), since $C_{z,\alpha} < 0$, due to the aerodynamic characteristic, both the terms η_A and η_T have the same sign. In addition, the control effectiveness related to the aerodynamic force (i.e., η_A) decreases as the operating altitude increases. Accordingly, the total control effectiveness varies from the endo- to exo-atmospheres as follows:

$$\eta = \eta_A + \eta_T \quad \rightarrow \quad \eta = \eta_T. \tag{21}$$

Note, this variation is smooth due to the decrease in dynamic pressure. Consequently, by utilizing the proposed control mechanism, it becomes possible to design an autopilot, which can be automatically and smoothly adjusted according to variations of the total control effectiveness caused by environmental changes in the transition from the endo-atmosphere to exo-atmosphere. As shown in Eq. (21), we can readily predict that the magnitude of the total control effectiveness in the endo-atmosphere is larger than in the exo-atmosphere. In other words, even a small change of the angle-of-attack can introduce a large change of the normal acceleration, in the endo-atmosphere. Thus, under this control mechanism, it can be readily predicted that the interceptor is operating at a low angle-of-attack regime in the endo-atmosphere and a high angle-of-attack regime in the exo-atmosphere. Note, this characteristic is beneficial in both the environmental regions. In the endo-atmosphere, a low angle-of-attack is good for reducing the aerodynamic drag. Whereas, in the exo-atmosphere, a high angle-of-attack does not create any issue concerning the aerodynamic drag because, in this flight region, the aerodynamic drag is negligible due to the loss of air density. Furthermore, in this region, allowing a high angle-of-attack is beneficial to attain a large normal acceleration.

In the next section, the proposed autopilot will be designed based on the control mechanism as discussed above.

Remark 2. In the derivation of Eq. (16), we utilize the fact that the terms with $\dot{\delta}_t$ are less dominant than the other terms due to the following reasons. First, in a real application, a guidance command is generally continuous and slowly-varying. Accordingly, the output of autopilot (i.e. δ_t) is also continuous and slowly-varying during a flight. Therefore, we can assume that the time-derivative of δ_t is small enough to be neglected when designing autopilots. Second, during the transition phase, $\dot{\delta}_t$ is relatively large. However, in the steady-state, $\dot{\delta}_t$ is very small. Therefore, neglecting the time-derivative of δ_t does not affect the steady-state performance in practice. This approximation is also verified through numerical simulations in Section V.

B. System Equation for Autopilot Design

Before delving into the autopilot design, the system equations for designing the proposed autopilot are discussed in this section. Since the normal acceleration a_z^w is chosen as the controlled output, utilizing the system equation in the terms of a_z^w, the so-called output dynamics, is beneficial. In this sense, substituting Eq. (11) into Eq. (17) yields

$$\dot{a}_z^w = \eta \left(\frac{a_z^w}{V} + q \right). \tag{22}$$

In addition, since the deflection angle of TVC (i.e., δ_t) is small in Eq. (4), the body pitch rate dynamics is approximated as

$$\dot{q} = \frac{q_\infty S_{ref} d_{ref} C_M}{I_{yy}} - \frac{l_t T \delta_t}{I_{yy}}. \tag{23}$$

Then, by combining Eqs. (22) and (23), the system equations for the proposed autopilot are constructed. In the system equations, the state variables are the normal acceleration and the body pitch rate. Also, the control input is the deflection angle of TVC. In the system equations, the body pitch rate dynamics Eq. (23) is usually much faster than the normal acceleration dynamics Eq. (22), because the body pitch rate dynamics is directly affected by the control input δ_t. Accordingly, based on the time-scale separation, the normal acceleration and the body pitch rate dynamics can be separated, thereby, allowing the utilization of a cascade structure with the inner loop and outer loop when designing the autopilot. Specifically, the acceleration feedback and the body pitch rate feedback constitute the outer loop and the inner loop, respectively. Hence, the two feedback loops can be separately designed. Note, the time-scale separation technique has been widely considered and accepted in missile autopilot designs [14], [18], [19], [22], [30]–[33]. Additionally, according to our recent work [14], it has been revealed that the well-known three-loop autopilot [19]–[21], [23]–[27] also has been developed based on the time-scale separation. Based on this aspect, the proposed autopilot design will follow this strategy as well.

In our previous work [14], a nonlinear autopilot design process based on the FBLC in conjunction with the time-scale separation was proposed for aerodynamic-controlled missiles, which rely on the moment control mechanism. In [14], it has been revealed that in case, the desired error dynamics for outer loop and inner loop are chosen as the first-order system and the second-order system, respectively. Correspondingly, under the FBLC, a resultant autopilot becomes a nonlinear version of the well-known three-loop missile autopilot. Since the three-loop missile structure has been well-understood over the past several decades, it can be beneficial for reliability. Also, through the elimination of the need for a tedious design process such as gain scheduling, the nonlinear autopilot design becomes more beneficial.

In order to exploit these benefits, the proposed autopilot will be designed using the approach in [14]. Since under the proposed control concept, the normal acceleration is also controlled by the moment control mechanism, the design process in [14] can be directly applied to the system equations as shown in Eqs. (22) and (23). Compared to [14], the mechanisms to generate moment (aerodynamic control fin $\rightarrow$ TVC) and the output variable (body acceleration $\rightarrow$ normal acceleration) are different.

Remark 3. Note, under the time-scale separation, there is no internal dynamics in the inner loop dynamics and the outer loop dynamics as shown in Eqs. (22) and (23) because the system dynamics and output dynamics have the same order.

Remark 4. The variations of dynamic pressure (or velocity) and mass are not considered in the proposed autopilot design since the dynamic pressure and mass are slowly varying parameters compared to other state variables. Also, since the variations of dynamic pressure and mass are not dominant parameters to induce normal acceleration, they can be neglected when designing autopilots from a practical perspective. This approximation will be verified in the numerical simulation. In other words, a high-fidelity longitudinal missile model including the variations of dynamic pressure and mass will be utilized to test the performance of the proposed autopilot, which is based on the simplified model as shown in Eqs. (22) and (23).

C. Feedback Loop Design for Normal Acceleration

In the feedback loop design for the normal acceleration, the output variable and the control input are considered as the normal acceleration and the body pitch rate, respectively. The acceleration feedback loop is used to calculate the body pitch rate command in order to achieve the desired normal acceleration command. Correspondingly, the system equation of the normal acceleration, as shown in Eq. (22), with the feedback linearization technique is used to design the acceleration feedback loop. In the feedback linearization technique, the choice of the desired error dynamics can determine the control structure and decide the overall control performance. In addition, it should be designed in consideration of the dynamic characteristics of system equations. In Eq. (22), a multiplicative modeling error is expected in practice and thus, the desired error dynamics for the normal acceleration is simply chosen as the first-order system. The desired error dynamics for the normal acceleration in the time domain can be written as:

$$\dot{a}_z^w - \frac{1}{\tau} \left(a_{z,c} - a_z^w \right) = 0. \tag{24}$$

where τ is the time constant of the first-order system, which can be considered as a design parameter of the acceleration feedback loop. In order to achieve this error dynamics, the control command of the acceleration feedback loop is determined by substituting Eq. (24) into Eq. (22) as follows:

$$q_c = \frac{1}{\tau\eta}\left(a_{z,c} - a_z^w\right) - \frac{a_z^w}{V}. \tag{25}$$

This command is given by the body pitch rate required to achieve the first-order response of the normal acceleration. In the next section, the body rate feedback loop design to achieve the desired value is described.

D. Feedback Loop Design for Body Pitch Rate

In the feedback loop design for the body pitch rate, the output variable and the control input are considered as the body pitch rate and the deflection angle of TVC, respectively. The main goal of this feedback loop is to generate the deflection angle command of TVC in order to achieve the desired body pitch rate from the outer loop (i.e., the feedback loop design for the normal acceleration). Similarly, the feedback linearization approach is applied to the dynamics equation of the body pitch rate, as shown in Eq. (23). In a real application, the aerodynamic uncertainties and the center of gravity uncertainties have been observed to induce the modeling errors in the body pitch rate dynamics. These modeling errors can be in the form of multiplicative modeling errors as well as additive modeling errors. Accordingly, the desired error dynamics of the body pitch rate is chosen as the second-order system as:

$$\dot{q} + 2\zeta\omega q + \omega^2 \int (q - q_c)\, dt = 0. \tag{26}$$

where ω and ζ denote the natural frequency and damping ratio of the rate feedback loop, respectively and are considered to be the design parameters. The parameter q_c represents the desired body pitch rate to be achieved, which is determined by the acceleration feedback loop, as shown in Eq. (25). Finally, the control command of the rate feedback loop is determined by substituting Eq. (26) into Eq. (23) as follows:

$$\delta_{t,c} = \frac{q_\infty S_{ref} d_{ref} C_M}{l_t T} - \frac{I_{yy}}{l_t T} 2\zeta\omega \left(\frac{\omega}{2\zeta}\int (q_c - q)\, dt - q\right). \tag{27}$$

This command can also be rewritten in terms of a trim command. In accordance with the definition of trim (i.e., $\dot{q} = 0$), the trim command can maintain the trim condition, which is determined from Eq. (23) with $\dot{q} = 0$:

$$\delta_{trim} \triangleq \frac{q_\infty S_{ref} d_{ref} C_M}{l_t T}. \tag{28}$$

By using the expression of the trim command, the control command of the rate feedback loop can also be rewritten as follows:

$$\delta_{t,c} = \delta_{trim} - \frac{I_{yy}}{l_t T} 2\zeta\omega \left(\frac{\omega}{2\zeta}\int (q_c - q)\, dt - q\right). \tag{29}$$

E. Discussion

In this section, the characteristics of the proposed autopilot are investigated. The control commands in Eqs. (25) and (29) can be rewritten as follows:

$$q_c = K_A\left(a_{z,c} - a_z\right) - K_{DC} a_z. \tag{30}$$

$$\delta_{t,c} = \delta_{trim} + \left(K_I \int (q_c - q)\, dt - q\right) K_R. \tag{31}$$

where

$$K_{DC} = \frac{1}{V}, \quad K_A = \frac{1}{\eta\tau}. \tag{32}$$

$$K_R = -\frac{2\zeta\omega I_{yy}}{l_t T}, \quad K_I = \frac{\omega}{2\zeta}. \tag{33}$$

From Eqs. (32) and (33), the new variables K_A and K_{DC} are defined to be the time-varying gains of the acceleration feedback loop, and the new variables K_I and K_R are considered as the time-varying gains of the rate feedback loop.

First, let us analyze the characteristic of the acceleration feedback loop with Eqs. (30) and (32). The control gains K_A and K_{DC} are automatically adjusted according to the variations of the speed and the environmental effectiveness factor η, and the effectiveness factor η changes in the endo- and exo-atmospheres, as shown in Eqs. (20) and (21). Specifically, the control gains K_A in the endo- and exo-atmospheres respectively are given as:

$$K_A = \frac{1}{\left(\frac{q_\infty S_{ref} C_{z,\alpha}}{m} - \frac{T}{m}\right)\tau}. \tag{34}$$

$$K_A = -\frac{m}{T\tau}. \tag{35}$$

It can be readily observed that the control gain K_A is automatically adjusted as the variations of the effectiveness of the aerodynamic force and the thrust. Accordingly, the magnitude of the control gains K_A gradually increases, as the control effectiveness η decreases from the endo- to exo-atmosphere. Also from Eq. (30), it can be observed that the control gain K_{DC} affects a steady-state error of the acceleration feedback loop and is adjusted by the speed of the interceptor. In addition, the response of the controller can be designed for the first-order system, which has the time constant as τ. Correspondingly, in order to obtain a fast response, the design parameter τ needs to be tuned as a small value. However, in this case, the time response of the acceleration feedback loop should be slower than that of the rate feedback loop.

Second, the characteristic of the body pitch rate loop with Eqs. (31) and (33) is analyzed. These control gains are characterized as the time-varying parameters by the aerodynamic coefficients, thrust, and missile configurations. Therefore, with the change in these parameters, the control gains K_I and K_R are automatically adjusted. In addition, the control gains K_I and K_R are also given by the functions of the design parameters ζ and ω, which determine the desired second-order response. When designing these parameters, the time response of the body pitch rate should be slower than that of the TVC actuator loop.

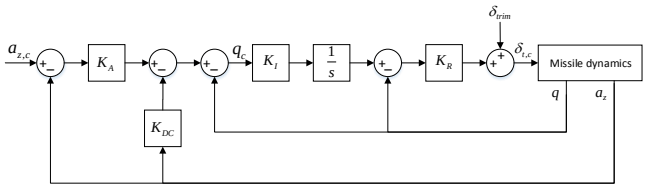

Fig. 2: The structure of proposed autopilot.

Fig. 2 represents the proposed autopilot structure which notably, is similar to the well-known three-loop autopilot [1], [14]–[18]. Also, the conventional three-loop autopilot (i.e., the linear three-loop autopilot) has the constant gain sets, and the gain-scheduling technique is normally used to operate in various flight conditions. Consequently, the specific gain sets are tuned in several flight conditions, and the gain sets are switched as flight conditions change during in-flight. However, the proposed nonlinear autopilot can adjust the control gains automatically with the change in the flight conditions. In other words, the control gains of the proposed nonlinear autopilot are automatically adjusted corresponding to the control effectiveness changes. Another difference is that the trim command δ_{trim} is added to the control command of the rate feedback loop as opposed to the conventional three-loop autopilot, and the trim command can help the transition performance of the autopilot improve by rapidly situating the autopilot near the operating point.

Besides, advantageously, the resultant autopilot is provided by a similar form of the well-known three-loop autopilot [1], [14]–[18]. Correspondingly, an autopilot designer may have confidence in the reliability of the proposed autopilot when implementing it in a real missile system, as the physical meaning or the working principle of the proposed controller can be clearly presented.

IV. Behavior of Tracking Error in Presence of Modelling Errors

In this section, the tracking error of the proposed autopilot is investigated for showing its characteristics of the plant parameter variations. In practice, since the dynamic equations are inaccurate due to model uncertainties such as aerodynamic uncertainties, thrust uncertainties, physical uncertainties, etc., obtaining an understanding and analyzing the behavior of the autopilot due to the plant parameter variations is an essential prerequisite for evaluating its reliability and predicting its performance. As such, the tracking error analysis in the presence of the plant parameter variations is performed to elucidate the relationship between the plant parameter variations and the stability margin in the nonlinear dynamic inversion autopilot.

In the proposed autopilot, the full knowledge of the dynamic model is required to generate the control commands. However, in a real application, the dynamic model may contain modeling errors due to the uncertainties of aerodynamic coefficients and missile parameters. In order to bridge this gap, in this section, the behavior of the tracking errors is determined in the presence of the modeling errors. In this analysis, it is assumed that the representative modeling errors are induced by the uncertainties of aerodynamic coefficients, thrust level, center of gravity, and moment of inertia. Then, from Eqs. (25) and (20), the body pitch rate command with the modeling errors is given as:

$$\hat{q}_c = \frac{m}{\tau\left(q_\infty S_{ref}\hat{C}_{z,\alpha} - \hat{T}\right)}\left(a_{z,c} - a_z^w\right) - \frac{1}{V}a_z^w. \tag{36}$$

where the parameter with a hat notation (i.e., $\hat{}$) represents the inaccurate model information. It is assumed that this is the best knowledge about the dynamic model in the autopilot design step. When this control command is applied, the closed-loop dynamics of the normal acceleration is determined by substituting Eq. (36) into Eq. (22).

$$\dot{a}_z^w = \frac{1}{\hat{\tau}}\left(a_{z,c} - a_z^w\right). \tag{37}$$

with

$$\hat{\tau} = \left(\frac{q_\infty S_{ref}\hat{C}_{z,\alpha} - \hat{T}}{q_\infty S_{ref}C_{z,\alpha} - T}\right)\tau. \tag{38}$$

In this case, the tracking error dynamics is also determined as

$$\dot{e}_1 = -\frac{1}{\hat{\tau}}e_1. \tag{39}$$

where $e_1 = a_{z,c} - a_z^w$. The tracking error dynamics is altered by the modeling errors. In Eq. (39), the parameters $\hat{\tau}$ and τ represent the achieved time constant and the desired time constant, respectively. As shown in Eq. (38), the modeling errors act as a scaling factor for the desired time constant. Namely, the modeling errors force the achieved time constant to vary from the desired value. When the model information is perfect, the achieved time constant is equal to the desired time constant as $\hat{\tau} = \tau$. As shown in Eq. (39), it is also noted that the tracking error converges to zero even in the presence of the modeling errors, which, in fact, only influence the convergence speed of the tracking error (i.e., the transient response in the acceleration feedback loop).

Next, from Eq. (27), the deflection angle command with the modeling errors can be expressed as

$$\hat{\delta}_{t,c} = \frac{q_\infty S_{ref} d_{ref}\hat{C}_M}{\hat{l}_t\hat{T}} - \left(\frac{\omega}{2\zeta}\int\left(q_c - q\right)dt - q\right)\frac{\hat{I}_{yy}}{\hat{l}_t\hat{T}}2\zeta\omega. \tag{40}$$

Under this control command, the closed-loop dynamics of the body pitch rate is determined by substituting Eq. (40) into Eq. (23)

$$\dot{q} = \hat{\omega}^2\int\left(q_c - q\right)dt - 2\hat{\zeta}\hat{\omega}q + \Delta. \tag{41}$$

with

$$\begin{aligned}\hat{\omega} &= \sqrt{\frac{\hat{I}_{yy}l_tT}{I_{yy}\hat{l}_t\hat{T}}}\omega, \qquad \hat{\zeta} = \sqrt{\frac{\hat{I}_{yy}l_tT}{I_{yy}\hat{l}_t\hat{T}}}\zeta, \\ \Delta &= \frac{q_\infty S_{ref} d_{ref} l_t T}{I_{yy}}\left(\frac{C_M}{l_tT} - \frac{\hat{C}_M}{\hat{l}_t\hat{T}}\right).\end{aligned} \tag{42}$$

By taking the time derivative of Eq. (41), the tracking error dynamics in the presence of the modeling errors is obtained as follows:

$$\ddot{e}_2 = -2\hat{\zeta}\hat{\omega}\dot{e}_2 + \hat{\omega}^2 e_2 + \dot{\Delta}. \tag{43}$$

where $e_2 = q_c - q$. The tracking error dynamics is also altered by the modeling errors. In Eq. (41), the parameters $\hat{\zeta}$ and $\hat{\omega}$ denote the achieved damping ratio and the achieved natural frequency. The parameters ζ and ω represent the desired damping ratio and the desired natural frequency. The parameter Δ represents a bias-type error. Because the modeling errors also act as scaling factors for the desired parameters in the pitch rate feedback loop. In this case, the modeling errors introduce the bias-type error as well. When the model information is perfect, we can achieve $\hat{\zeta} = \zeta$, $\hat{\omega} = \omega$, and $\Delta = 0$, respectively. In Eq. (43), if the bias-type error is slowly varying (i.e., $\dot{\Delta} \approx 0$), the tracking error dynamics can be approximated as

$$\ddot{e}_2 = -2\hat{\zeta}\hat{\omega}\dot{e}_2 + \hat{\omega}^2 e_2. \tag{44}$$

In this case, the tracking error converges to zero even in the presence of the modeling errors, which similarly, only affect the convergence pattern of the tracking error. However, in the case of $\dot{\Delta} \neq 0$, it is expected that the modeling errors might also influence the steady-state performance due to the bias-type error.

Remark 5. Note, the purpose of this analysis is to show a general insight into the behavior of nonlinear autopilot in the presence of the modeling errors. In this context, the simplifications (i.e., the time-scale separation) have been considered to make the analysis tractable for the analysis purpose. Therefore, in case, the absolute time-scale separation and perfect tracking are not valid, the analysis results might not represent the system responses correctly. However, the proposed control mechanism maintains the time-scale separation because the pitch rate dynamics are sufficiently fast under the proposed control mechanism.

V. Numerical Simulation Results

This section presents the numerical simulation results in order to verify the proposed autopilot. The initial mass of the missile is 1000 kg, and the total mass decreases continuously due to fuel consumption. In practice, the current mass information could be obtained by a mass model. Also, the mass flow rate of the thruster is assumed as 9.35 kg/s, and burn time is set to 80 s. In addition, the actuator model, which is included in the simulation is given as:

$$G_a(s) = \frac{\omega_a^2}{s^2 + 2\zeta_a\omega_a + \omega_a^2} \left(\omega_a = 15Hz, \zeta_a = 0.707\right). \tag{45}$$

Moreover, the proposed autopilot is designed to satisfy the following performance.

- Gain margin $>$ 6 dB
- Phase margin $>$ 45 deg
- Rise time of the acceleration loop $<$ 0.5 s
- The acceleration command $<$ 6 g

In order to analyze the response at each altitude, the mass, speed, and thrust are obtained from the reference trajectory as shown in Table I.

TABLE I: The initial conditions at each altitude.

Altitude [km]	0	10	20	30	50	60
Mass [kg]	1000	713.4	589.8	503.1	381.6	335.1
Thrust [G]	2.52	3.54	4.28	5.02	6.62	7.53
Speed [Mach]	0.06	2.4	3.6	4.9	7.3	8.5

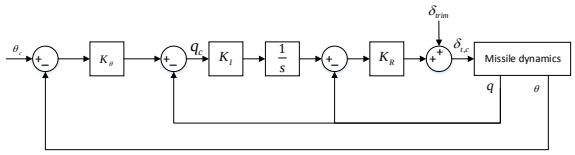

(a) Conventional pitch controller.

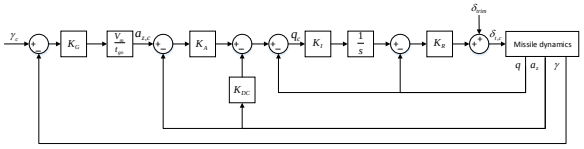

(b) Normal acceleration (flight path angle) controller.

Fig. 3: Designed controllers for analysis of aerodynamical mechanism.

A. Investigation of the aerodynamic mechanism

As mentioned before, the angle of attack is rapidly converged to zero with the aerodynamic effect, and the flight path angle is converged to the pitch angle rapidly. That is because the air density is high at the low altitude, and the time response of the flight path angle control rapidly increases. Therefore, in case, the rate of convergence of the angle of attack is fast enough, we can utilize the attitude controller to adjust the flight path angle. In this manner, the attitude controller can control the flight path angle, indirectly. In addition, the flight path angle is difficult to obtain whereas, the attitude angle can be directly calculated by an inertial navigation system in practice. For this reason, the autopilot of the conventional interceptor is designed as the attitude control scheme at a low altitude. However, the autopilot, which adopts the attitude as the control parameter, has a critical disadvantage at the high altitude. In order to investigate the aerodynamic mechanism at the low and high altitude, we designed the conventional pitch angle controller and the flight path angle controller as shown in Fig. 3.

In order to compare under the same condition, the initial speed and mass were set at 1000 m/s and 200 kg, respectively. As shown in Fig. 4 (a), the time responses of the pitch angle at various altitudes are the same whereas, the time responses of the flight path angle become slower at the high altitude. From the result, it can be deduced that the performance of the attitude controller is degraded at the high altitude clearly.

The phenomenon occurs because the angle-of-attack converges to zero slowly at a high altitude. Similarly, the angle-of-attack at the high altitude is larger than the angle-of-attack at the low altitude, as shown in Fig. 4 (b). In addition, it means that a large angle-of-attack at the high altitude is required to obtain the same amount of the control force that is required at the low altitude. As a result, it takes more time for the angle-of-attack to converge to zero. For this reason, the performance

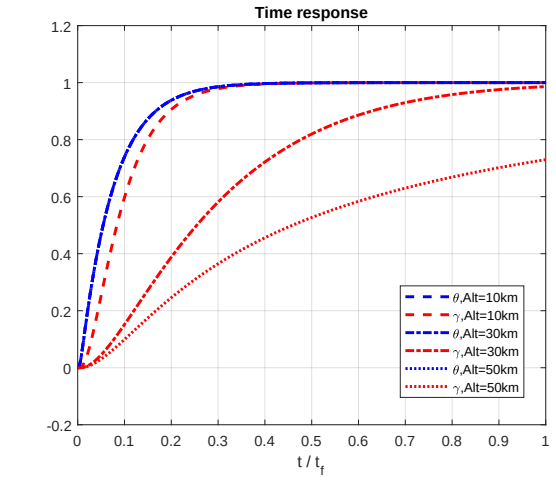

(a) Time response of attitude controller.

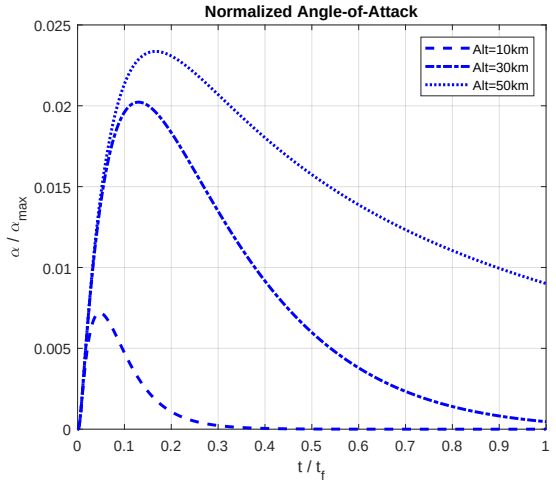

(b) Normalized angle of attack.

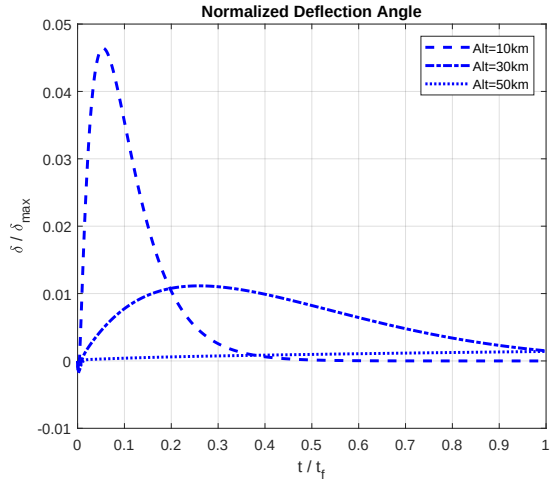

(c) Normalized deflection angle.

Fig. 4: Performance analysis with attitude control scheme at each altitude.

of the autopilot with the attitude control structure decreases significantly at the high altitude. Although the time responses are the same at three attitudes, the required deflection angles decrease at the high altitudes, as shown in Fig. 4 (c). That is because the required aerodynamic drag is also reduced at the high altitude, and the small amount of deflection angle could be affordable to induce the same effect.

B. Investigation of basic properties

In order to investigate the basic property of the proposed autopilot, nonlinear simulations were performed and the initial conditions are presented in Table I, and the required acceleration command was 2 g. The normal accelerations are shown in Fig. 5 (a), which shows that although the control structure was the same at all altitudes, the response of the normal acceleration was generated uniformly. In addition, the circle markers in Fig. 5 (a) showed a 0 - 90% rise time at each altitude condition. The rise time at each altitude was under 0.5 s, which is the requirement of the designed controller.

Moreover, Fig. 5 (b) depicts the normalized deflection angle of TVC at various altitudes. The deflection angle command decreased at the high altitude and this trend could be attributed to the nullification of the aerodynamic moments. In the endo-atmospheric region, an additional deflection angle was required to nullify the aerodynamic moments for maintaining the trim condition. However, in the exo-atmospheric region, the deflection angle for maintaining the trim condition decreased, due to the decrease in the effectiveness of the aerodynamic forces. Moreover, the deflection angles above 50 km became nearly zero.

The normalized angle-of-attack at various altitudes are shown in Fig. 5 (c). The angle-of-attack was less at low altitudes, which means that even a small angle-of-attack in the endo-atmospheric region can generate adequate normal acceleration due to the large aerodynamic force. On the contrary, in the exo-atmospheric region, a relatively small and limited thrust required a high angle-of-attack to produce the same amount of the normal acceleration as that produced in the endo-atmospheric region.

Furthermore, the control effectiveness of the thrust is shown in Fig. 5 (d), illustrating that the effectiveness of thrust is automatically adjusted to a high value at a high altitude. It implies that the thrust becomes the dominant control force at high altitudes.

C. Robustness study of proposed autopilot

1) Relative stability analysis: In order to investigate the robustness of the proposed controller, the relative stability is analyzed in this subsection. According to the well-known control theory, the robustness against the perturbations can be addressed by determining the relative stability, and this is widely accepted in practice. The relative stability can be considered as the information on how stable a control loop is, and specifically, the relative stability is represented as the gain margin and the phase margin from the linear control theory. In the nonlinear dynamic inversion, it is difficult to address the gain margin and the phase margin as well as

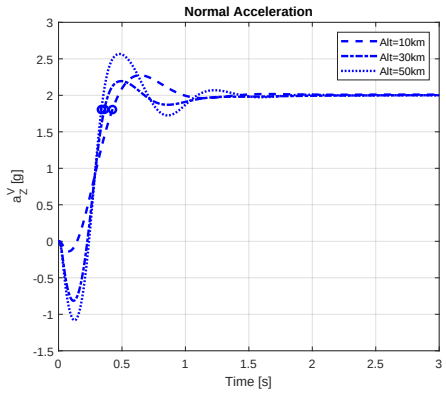

(a) Normalized acceleration.

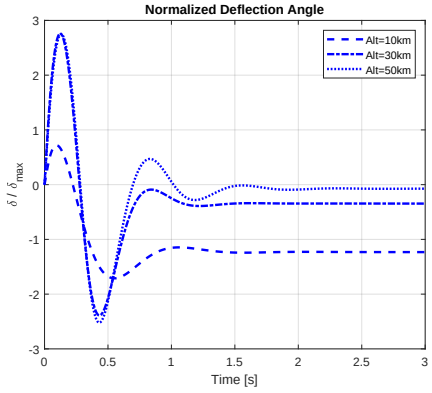

(b) Normalized deflection angle of TVC.

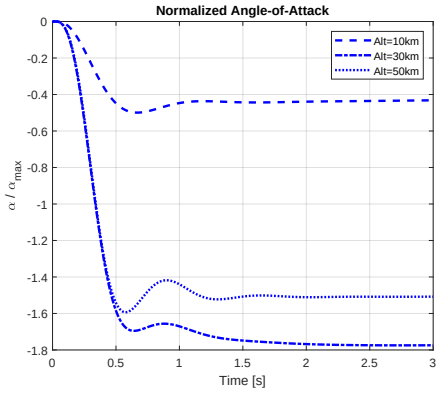

(c) Normalized angle-of-attack.

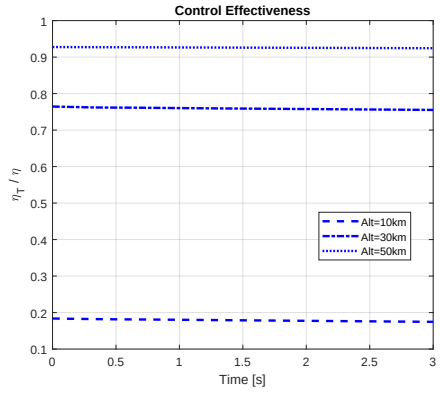

(d) Control effectiveness.

Fig. 5: Basic performance analysis with 2 g command.

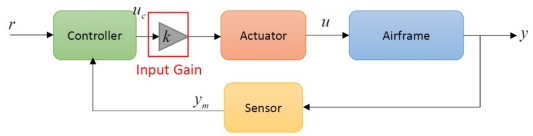

(a) The method to determine the gain margin.

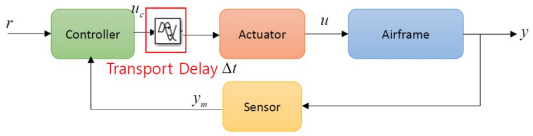

(b) The method to determine the phase margin.

Fig. 6: Relative stability analysis for the proposed controller.

there are no rigorous theories. Therefore, as in [34], we utilized a practical approach: To determine the gain margin and the phase margin using their physical meanings. The gain margin is physically the amount of allowable gain increase while maintaining control loop stability. Namely, the physical meaning of the gain margin is the amount of permissible modeling error. Therefore, the gain margin of the nonlinear dynamic inversion autopilot can be numerically determined based on its physical meaning as follows:

- Put an input gain k before actuator as shown in Fig. 6 (a), and find maximum value k until control loop becomes unstable.
- Once we find the maximum value k, we can compute the gain margin as

$$GM = 20\log_{10}(k) \ [\text{dB}]. \tag{46}$$

The phase margin is the amount of allowable phase shift while maintaining control loop stability. Therefore, the physical meaning of the phase margin can be considered as the amount of allowable time delay in the control loop. Therefore, the phase margin of the nonlinear dynamic inversion autopilot can be numerically determined based on its physical meaning as follows:

- Impose a transport delay Δt before actuator as shown in Fig. 6 (b), and find maximum Δt until the control loop becomes unstable. Herein, Δt can be considered as the time delay margin.
- Compute the gain-crossover frequency f from the obtained response (read frequency from oscillation response).
- Compute the phase margin as follows:

$$PM = 360 f \Delta t [deg]. \tag{47}$$

By using these approaches, we performed the robustness analysis as presented in Figs. 7 and 8, and the gain margin and phase margin satisfied the design criteria; Gain margin $>$ 6 dB and Phase margin $>$ 45 deg.

2) Uncertainty of Aerodynamic force and thrust: The proposed control structure utilizes the aerodynamic force and thrust to obtain the control gains, and it is similar to the dynamic inversion technique. This correspondingly implies that in case, the parameters of the aerodynamic force and thrust have errors, the controller could be unstable. Given this perspective, Figs. 9-11 depict the simulation results to verify

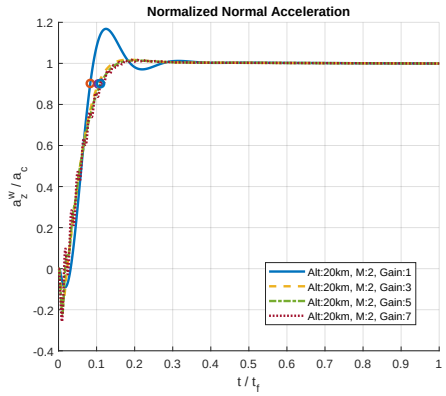

(a) Mach:2 and altitude:20km.

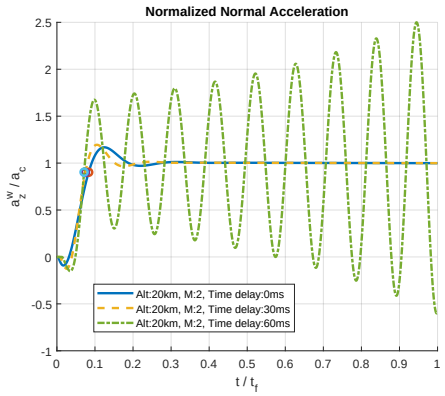

(a) Mach:2 and altitude:20km.

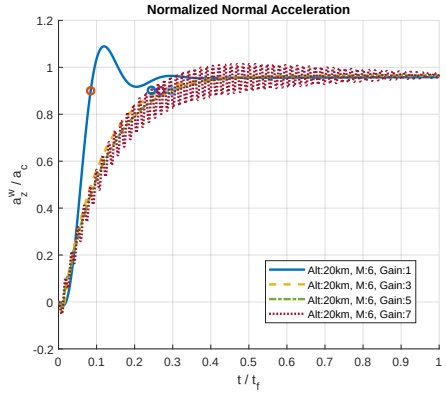

(b) Mach:6 and altitude:20km.

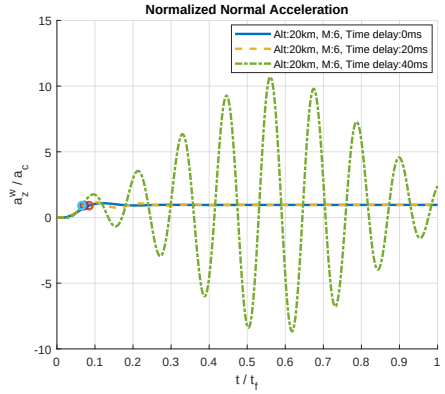

(b) Mach:6 and altitude:20km.

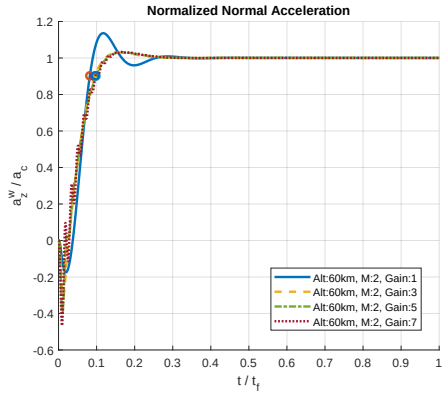

(c) Mach:2 and altitude:60km.

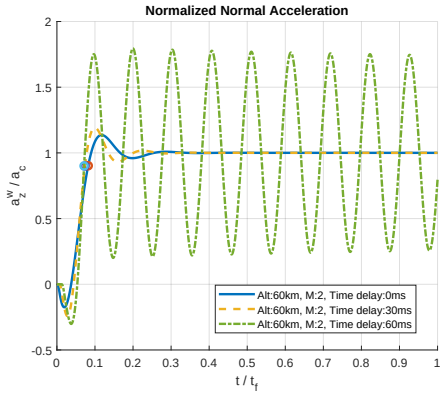

(c) Mach:2 and altitude:60km.

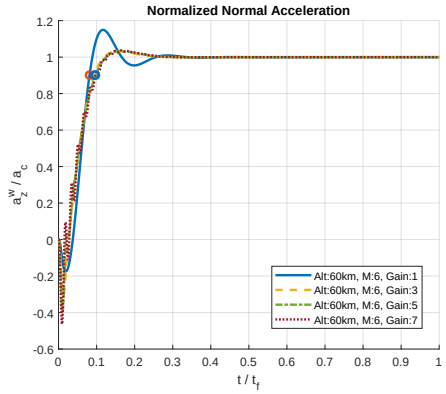

(d) Mach:6 and altitude:60km.

Fig. 7: Relative stability analysis with gain margin.

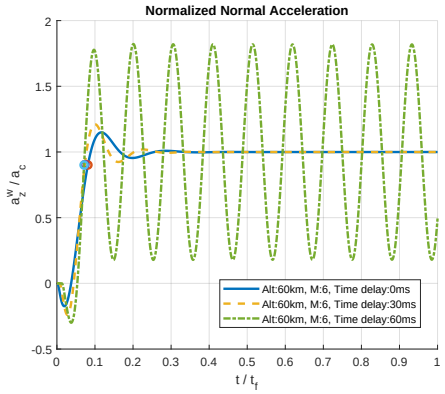

(d) Mach:6 and altitude:60km.

Fig. 8: Relative stability analysis with phase margin.

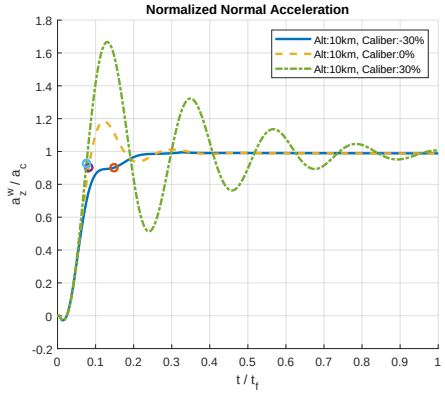

(a) Altitude:10km and CP:$\pm 30\%$.

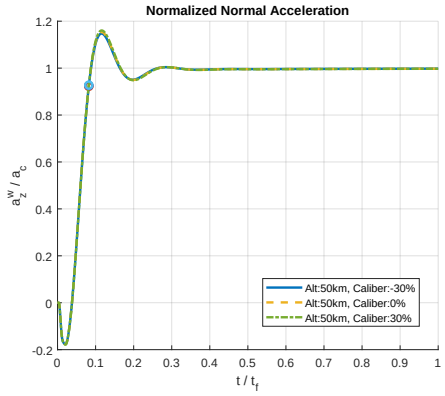

(b) Altitude:50km and CP:$\pm 30\%$.

Fig. 9: Relative stability analysis with center of pressure(CP) uncertainty.

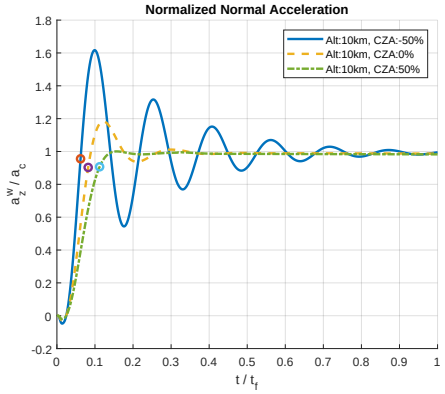

(a) Altitude:10km and C_{z_α} : $\pm 50\%$.

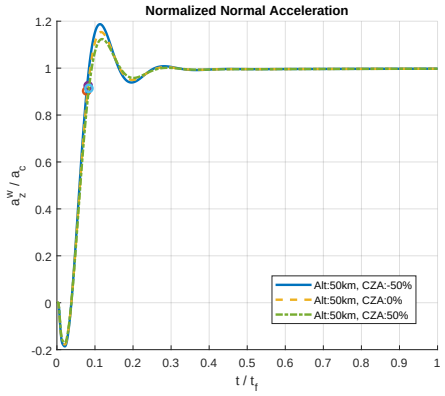

(b) Altitude:50km and C_{z_α} : $\pm 50\%$.

Fig. 10: Relative stability analysis with C_{z_α} uncertainty.

the robustness of the controller under the modeling errors. In practice, it is difficult to obtain the exact information on the center of pressure, the aerodynamic coefficient C_{z_α}, and thrust profile. Therefore, it is assumed that the center of pressure, C_{z_α}, and thrust have errors in the simulation. At the low altitude, these uncertainties can affect the response directly. In contrast, at the high altitude, the uncertainties can induce less effect on its stability as the aerodynamic drag and moment vanish at the high altitude.

D. Engagement simulation

In order to verify the proposed control structure, the engagement simulation was performed as shown in Fig. 12, and for the comparison to the existing approach, a switching mechanism was utilized to the simulation. The controller was switched from the conventional pitch controller to the normal acceleration controller at 20 km, and the gains of the controllers were tuned at several trim points and used by the gain scheduling algorithm. As shown in Fig. 12 (a), the trajectories of two approaches are found to be similar, but the performance of the attitude controller is attenuated near the switching points as shown in Fig. 12 (b). Contrariwise, the proposed approach depicts good tracking performance. Moreover, the required deflection angle of the switching approach is larger than that of the proposed approach as shown in Fig. 12 (c). From those results, the proposed approach shows a robust performance at entire altitude regions.

VI. Conclusion

This paper proposed a novel autopilot, without changing the control mechanism or the configuration of the control structure, for the interceptor with TVC, using the nonlinear control approach. The proposed autopilot can operate with the same control structure from the endo-atmospheric region to the exo-atmospheric region. In addition, since the proposed autopilot can be rearranged into the structure of the well-known three loop autopilot, the physical meaning of control commands can be analyzed intuitively. It implies that the proposed autopilot can be regarded as a proven controller in the real field. The tracking error of the proposed autopilot was analyzed in consideration of the modeling errors, and the relative stability was investigated by studying the robustness against the perturbations. The proposed autopilot shows the robust performance in the endo- and exo-atmospheric regions while changing the altitudes, as its performance was verified by the engagement simulation results between 0-50 km. The proposed autopilot can be utilized effortlessly for all kinds of aerial vehicles, which operate at various altitude ranges, such as high-altitude long-endurance aerial vehicles and rockets.

References

[1] P. B. Jackson, "Overview of missile flight control systems," *Johns Hopkins APL Technical Digest*, vol. 29, no. 1, pp. 9–24, 2010.

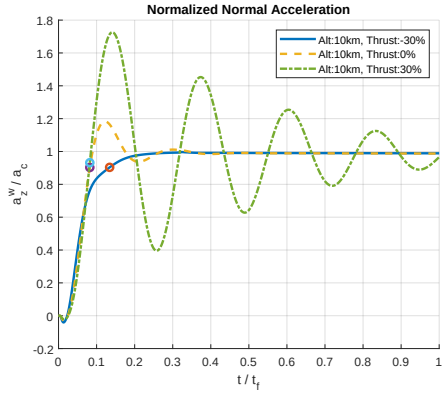

(a) Altitude:10km and thrust:±30%.

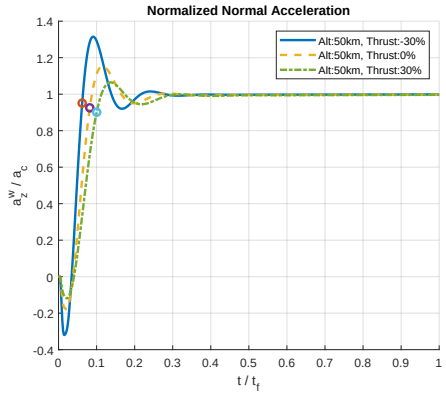

(b) Altitude:50km and thrust:±30%.

Fig. 11: Relative stability analysis with thrust uncertainty.

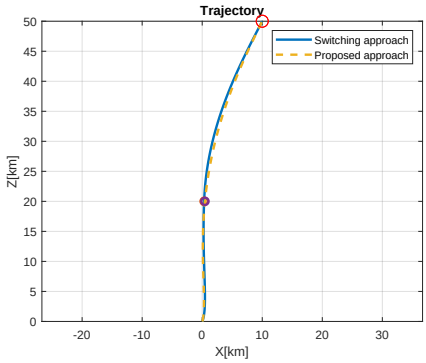

(a) Flight trajectory.

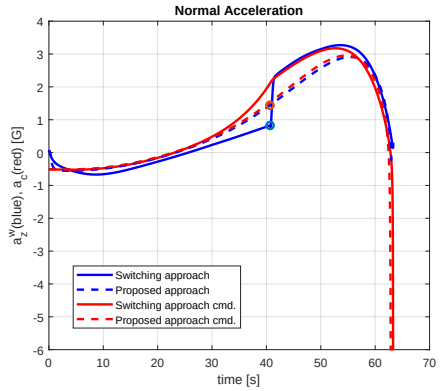

(b) Normal acceleration.

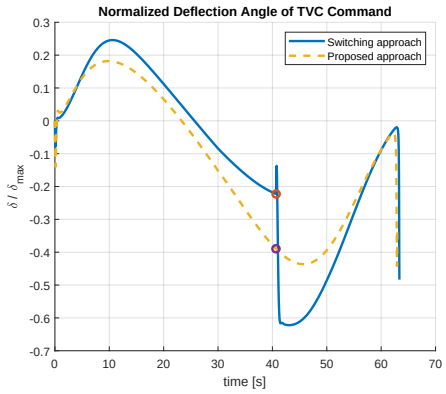

(c) Normalized deflection angle $\delta_{max} = 10deg$.

Fig. 12: Engagement simulation results.

[2] D. Foreman, C. Tournes, and Y. Shtessel, "Interceptor Missile Control-A New Look at Boost and Midcourse," in *AIAA Guidance, Navigation, and Control Conference*, 2010, p. 7579.

[3] F. K. Yeh, H. H. Chien, and L. C. Fu, "Design of optimal midcourse guidance sliding-mode control for missiles with TVC," *IEEE Transactions on Aerospace and Electronic Systems*, vol. 39, no. 3, pp. 824–837, 2003.

[4] Q. Zhi and Y.-L. Cai, "Energy-Management Steering Maneuver for Thrust Vector-Controlled Interceptors," *Journal of Guidance, Control, and Dynamics*, vol. 35, no. 6, pp. 1798–1804, 2012.

[5] T. Shima and O. M. Golan, "Exo-atmospheric guidance of an accelerating interceptor missile," *Journal of the Franklin Institute*, vol. 349, no. 2, pp. 622–637, 2012.

[6] S. Gutman and S. Rubinsky, "Exoatmospheric Thrust Vector Interception Via Time-to-Go Analysis," *Journal of Guidance, Control, and Dynamics*, vol. 39, no. 1, pp. 86–97, 2016.

[7] R. Tekin, O. Atesoglu, and K. Leblebicioglu, "Flight control algorithms for a vertical launch air defense missile," in *Advances in Aerospace Guidance, Navigation and Control*. Springer, 2013, pp. 73–84.

[8] S. R. Wassom, L. C. Faupell, and T. Perley, "Integrated aerofin/thrust vector control for tactical missiles," *Journal of Propulsion and Power*, vol. 7, no. 3, pp. 374–381, 1991.

[9] R. L. Eberhardt and K. A. Wise, "High gain H∞ feedback control for an anti-air missile," in *Proceedings of 32nd IEEE Conference on Decision and Control*, 1993, pp. 449–455.

[10] H. C. Lee, Y. S. Choi, and J. W. Choi, "Autopilot Design for Agile Missile Using Time-Varying Control Technique," vol. 37, no. 6. Elsevier, 2004, pp. 665–670.

[11] Y. B. Shtessel and C. H. Tournes, "Integrated Higher-Order Sliding Mode Guidance and Autopilot for Dual Control Missiles," *Journal of Guidance, Control, and Dynamics*, vol. 32, no. 1, pp. 79–94, 2009.

[12] Raziye Tekin, "Design, Modeling, Guidance and Control of a Vertical Launch Surface to Air missile," Ph.D. dissertation, Middle East Technical University, 2010.

[13] C.-H. Lee, B.-E. Jun, H.-S. Shin, and A. Tsourdos, "Nonlinear acceleration controller for exo-atmospheric and endo-atmospheric interceptors with TVC," in *2017 25th Mediterranean Conference on Control and Automation (MED)*. IEEE, 2017, pp. 153–157.

[14] C.-H. Lee, B.-E. Jun, and J.-I. Lee, "Connections Between Linear and Nonlinear Missile Autopilots via Three-Loop Topology," *Journal of Guidance, Control, and Dynamics*, vol. 39, no. 6, pp. 1426–1432, 2016.

[15] E. Devaud, J.-P. Harcaut, and H. Siguerdidjane, "Three-Axes Missile Autopilot Design: From Linear to Nonlinear Control Strategies," *Journal of Guidance, Control, and Dynamics*, vol. 24, no. 1, pp. 64–71, 2001.

[16] R. Padhi, C. H. V. Sirisha, A. K. Sarkar, P. K. Kar, and T. Srinivasan, "Nonlinear and Linear Autopilot Performance Comparison of Tactical Flight Vehicle," in *AIAA Guidance, Navigation, and Control Conference*, 2012, p. 4683.

[17] C. Hai-rong and Z. Yue, "Three-loop autopilot design and simulation," in *2012 IEEE International Conference on Mechatronics and Automation*, 2012, pp. 2499–2503.

[18] C.-H. Lee, B.-E. Jun, J.-I. Lee, and M.-J. Tahk, "Nonlinear missile autopilot design via three loop topology and time-delay adaptation scheme," in *2013 13th International Conference on Control, Automation*

and Systems (ICCAS 2013), 2013, pp. 50–54.
[19] M. A. Abd-elatif, L. jun Qian, and Y. ming Bo, "Optimization of three-loop missile autopilot gain under crossover frequency constraint," *Defence Technology*, vol. 12, no. 1, pp. 32–38, 2016.
[20] F. W. Nesline and N. C. Nabbefeld, "Design of digital autopilots for homing missiles," in *AGARD conference*, 1979, pp. 1–14.
[21] F. W. Nesline and M. L. Nesline, "How autopilot requirements constrain the aerodynamic design of homing missiles," in *American Control Conference, 1984*. IEEE, 1984, pp. 716–730.
[22] E. Devaud, H. Siguerdidjane, and S. Font, "Some control strategies for a high-angle-of-attack missile autopilot," *Control Engineering Practice*, vol. 8, no. 8, pp. 885–892, 2000.
[23] C. Mracek and D. Ridgely, "Missile longitudinal autopilots: connections between optimal control and classical topologies," in *AIAA guidance, navigation, and control conference and exhibit*, 2005, p. 6381.
[24] J.-L. Wang and Z.-K. QI, "Analysis of a three-loop autopilot," *Transactions of Beijing Institute of technology*, vol. 3, 2006.
[25] I. Rusnak, H. Weiss, and I. Barkana, "Improving the performance of existing missile autopilot using simple adaptive control," *IFAC Proceedings Volumes*, vol. 44, no. 1, pp. 6567–6572, 2011.
[26] P. Zarchan, *Tactical and strategic missile guidance*. American Inst. of Aeronautics and Astronautics, 2012.
[27] J.-H. Kim and I. H. Whang, "Augmented three-loop autopilot structure based on mixed-sensitivity h ∞ optimization," *Journal of Guidance, Control, and Dynamics*, vol. 41, no. 3, pp. 751–756, 2017.
[28] R. Padhi and M. Kothari, "Model predictive static programming: a computationally efficient technique for suboptimal control design," *International journal of innovative computing, information and control*, vol. 5, no. 2, pp. 399–411, 2009.
[29] S. He and C.-H. Lee, "Gravity-turn-assisted optimal guidance law," *Journal of Guidance, Control, and Dynamics*, vol. 41, no. 1, pp. 171–183, 2017.
[30] P. Menon and M. Yousefpor, "Design of nonlinear autopilots for high angle of attack missiles," in *Guidance, Navigation, and Control Conference*, 1996, p. 3913.
[31] E. Devaud, H. Siguerdidjane, and S. Font, "Nonlinear dynamic autopilot design for the non-minimum phase missile," in *Decision and Control, 1998. Proceedings of the 37th IEEE Conference on*, vol. 4. IEEE, 1998, pp. 4691–4696.
[32] M. B. McFarland and A. J. Calise, "Neural networks and adaptive nonlinear control of agile antiair missiles," *Journal of Guidance, Control, and Dynamics*, vol. 23, no. 3, pp. 547–553, 2000.
[33] S.-H. Kim, Y.-S. Kim, and C. Song, "A robust adaptive nonlinear control approach to missile autopilot design," *Control engineering practice*, vol. 12, no. 2, pp. 149–154, 2004.
[34] S.-H. Kim and M.-J. Tahk, "Missile acceleration controller design using proportionalintegral and non-linear dynamic control design method," *Proceedings of the Institution of Mechanical Engineers, Part G: Journal of Aerospace Engineering*, vol. 226, no. 8, p. 882897, 2011.

Ju-Hyeon Hong received the B.S., M.S., and Ph.D. degrees in aerospace engineering from Inha University, Incheon, Korea, in 2011, 2013, and 2017 respectively. Ju-Hyeon joined the Centre for Autonomous and Cyber-Physical Systems at Cranfield University as a Research Fellow in Aerospace Systems in 2017. Her research interests include the guidance, navigation, and control system for missiles and UAVs.

Chang-Hun Lee received the B.S., M.S., and Ph.D. degrees in aerospace engineering from the Korea Advanced Institute of Science and Technology, Daejeon, Korea, in 2008, 2010, and 2013, respectively. From 2013 to 2015, he was a Senior Researcher for Guidance and Control (G&C) Team, Agency for Defense Development, Daejeon, Korea. From 2016 to 2018, he was a Research Fellow for School of Aerospace, Transportaion, and Manufacturing, Cranfield University, Bedford, United Kingdom. Since 2019, he has been with the Department of Aerospace Engineering, Korea Advanced Institute of Science and Technology, Daejeon, Korea, where he is currently an Assistant Professor. His recent research interests include advanced missile guidance and control, cooperative control for unmanned aerial vehicles, target tracking filter, deep learning, and aviation data analytics.